THE JOURNAL OF PHYSICAL CHEMISTRY Letters

Letter

pubs.acs.org/JPCL

Following [FeFe] Hydrogenase Active Site Intermediates by Time-Resolved Mid-IR Spectroscopy

Mohammad Mirmohades,[#,∇] Agnieszka Adamska-Venkatesh,[‡,∇] Constanze Sommer,[‡] Edward Reijerse,[‡] Reiner Lomoth,[#] Wolfgang Lubitz,[*,‡] and Leif Hammarström[*,#]

[#]Department of Chemistry - Ångström Laboratory, Uppsala University, Box 523, 751 20 Uppsala, Sweden

[‡]Max Planck Institute for Chemical Energy Conversion, Stiftstrasse 34-36, 45470 Mülheim an der Ruhr, Germany

Supporting Information

ABSTRACT: Time-resolved nanosecond mid-infrared spectroscopy is for the first time employed to study the [FeFe] hydrogenase from *Chlamydomonas reinhardtii* and to investigate relevant intermediates of the enzyme active site. An actinic 355 nm, 10 ns laser flash triggered photodissociation of a carbonyl group from the CO-inhibited state H_{ox}-CO to form the state H_{ox}, which is an intermediate of the catalytic proton reduction cycle. Time-resolved infrared spectroscopy allowed us to directly follow the subsequent rebinding of the carbonyl, re-forming H_{ox}-CO, and determine the reaction half-life to be $t_{1/2} \approx 13 \pm 5$ ms at room temperature. This gives direct information on the dynamics of CO inhibition of the enzyme.

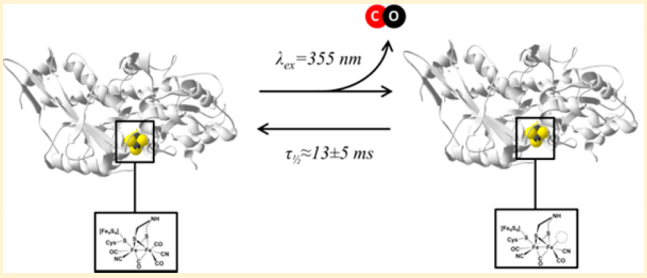

[FeFe] hydrogenases are the most efficient proton-reducing enzymes with turnover frequencies (TOFs) of up to several thousand per second.[1] Much work has been devoted to understanding the mechanisms of their operation and of competing inhibitory reactions.[2] Detailed understanding and comparison of hydrogenases from different organisms is of fundamental interest and may also guide efforts toward photobiological and photochemical hydrogen production using engineered microorganisms or bioinspired molecular catalysts.[3−18] The high maximum TOF of these enzymes warrants the need for transient techniques that are on the same time scale or faster, so that transient intermediates of the catalytic cycle can be resolved.[19] Until now, only equilibrium states have been detected under nonturnover conditions, and many measurements have been performed at very low temperatures, which is far from the physiological conditions under which these enzymes operate.[2,20] Time-resolved spectroscopic techniques may both resolve the kinetics between the known equilibrium states as well as discover new transient intermediates.

The current study was performed on an [FeFe] hydrogenase originating from *Chlamydomonas reinhardtii* (CrHydA1), which was obtained by overexpressing the apoenzyme in *Escherichia coli*[21] and subsequent artificial maturation with a synthetic cofactor.[22,23] To follow the intermediates of CrHydA1 transiently, the sample was excited with a laser pulse (fwhm: 10 ns; λ: 355 nm) to trigger photodissociation of a carbonyl group from a CO-inhibited state "H_{ox}-CO" and generate a state, "H_{ox}", that is part of the catalytic cycle. The released carbon monoxide then rebinds to the H_{ox} state to re-form the CO-inhibited state H_{ox}-CO. The reaction is followed with transient absorption spectroscopy at room temperature using mid-IR laser light, which is an excellent technique to follow changes of the 3−4 carbonyl and 2 cyanide ligands in the active site. The FTIR spectra of most of the states are known, which allows for safe assignments.[24,25]CO inhibition of [FeFe] hydrogenases and its relation to O_2 inactivation have been investigated with voltammetry and spectroscopic methods, which do not give direct information on the CO binding dynamics.[20,26−28] Research on specific CO binding dynamics of enzymes has in the past involved proteins with a heme group, such as cytochrome c and myoglobin. Step-scan FTIR measurements have been used to obtain information on their CO dissociation after photolysis.[29,30] We know of no step-scan FTIR studies of CO binding and inhibition in hydrogenases. This might be due to the limitation of the step-scan technique requiring a sample that is stable during $>10^4$ laser flashes and that give rise to large signals.[31] In the present work, we instead measure the kinetics in single-wavenumber traces using an average of only ∼10 laser flashes. This method has recently been used to study intermediates of a [NiFe] hydrogenase (TOF = 62 s^{-1}) following laser-flash generation of reducing equivalents.[32]

Because the measurements were performed at ambient, anaerobic conditions in an aqueous solution, they reflect the natural behavior of the enzyme. Water absorbs well in the mid-IR region, and therefore, the thickness of the IR cell was chosen to be only 50 μm. This also means that a high concentration of CrHydA1 was needed to have sufficient absorption to observe the changes occurring after excitation. The concentration of CrHydA1 was chosen to be 2.5 mM in all measurements.

Received: June 14, 2016
Accepted: August 5, 2016
Published: August 5, 2016

DOI: 10.1021/acs.jpclett.6b01316
J. Phys. Chem. Lett. 2016, 7, 3290−3293

A steady-state mid-FTIR spectrum was obtained before and after the 355 nm light excitation experiments, showing no significant changes after flashing with 355 nm light (Figure S1). When overlapping the H_{ox}-CO steady-state spectrum with the transient spectrum (Figure 1), there is perfect correspondence between the bleach features in the transient spectrum (in black) and the peaks in the steady-state spectrum (in red), showing that by flashing the sample a reversible chemical conversion is occurring. The infrared detection capabilities are limited to 1765−1925 and 1960−2150 cm^{-1}, and there is therefore a gap (1925−1960 cm^{-1}) where detection is not possible, which precludes detection of the H_{ox} state at 1940 cm^{-1}. Note that the other two carbonyl peaks of the H_{ox} state also cannot be detected; the 1964 cm^{-1} peak is overlapping with a peak in the H_{ox}-CO-inhibited state spectrum, making it impossible to detect it in a difference spectrum, and the 1800 cm^{-1} peak is smaller and overlapping with water vapor peaks that reduce the probe light intensity. The cyanide peaks between 2070 and 2100 cm^{-1} show relatively small and unspecific shifts upon changing the state of the active site and are therefore poor probes. Replacing the ^{12}CO with ^{13}CO in the [FeFe] hydrogenase shifts the whole carbonyl spectrum by ∼45 cm^{-1} to lower wavenumbers.[25] This should then shift the 1940 cm^{-1} peak to 1895 cm^{-1}, which is well within the detection range (note that the other two peaks will still not be able to be detected). The ^{13}CO-labeled H_{ox} state was indeed observed for the first time with a peak at 1894 cm^{-1}.

In Figure 2, the kinetic traces of the H_{ox}-^{12}CO-inhibited state spectrum as well as the H_{ox}-^{13}CO-inhibited states are plotted. The traces show that at around 200 μM, around 8% of the total sample is converted into H_{ox} after flashing with 355 nm light. A simple calculation shows that ∼10^{-9} mol of the enzyme is converted to the H_{ox} state after flashing, while about 1 order of magnitude more photons are absorbed by the sample (10^{-8} mol). This means that the quantum yield of conversion is around 10% for this enzyme. The kinetic traces also show that the photoinduced decarbonylation is a reversible process, that is, it is followed by a CO rebinding process with a half-life of $t_{1/2} \approx 13 \pm 5$ ms; see Figures 2 and S4.

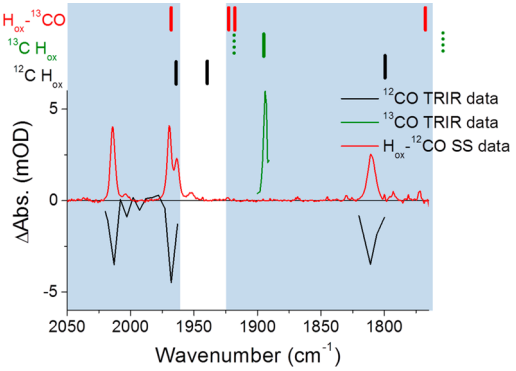

Figure 1. Time-resolved infrared (TRIR) transient absorption data after averaging data points 1−3 ms after excitation (laser excitation fwhm: 10 ns; λ: 355 nm). Black spectrum: 2.5 mM ^{12}CO-labeled CrHydA1 in the H_{ox}-CO-inhibited state. Green spectrum: 2.5 mM ^{13}CO-labeled CrHydA1 in the H_{ox}-CO-inhibited state. Red spectrum: Steady-state (SS) spectrum of 2.5 mM ^{12}CO-labeled CrHydA1 in the H_{ox}-CO-inhibited state. The carbonyl bands of H_{ox}-^{13}CO and ^{12}CO-labeled H_{ox} (from refs 24 and 25) as well as those for ^{13}CO-labeled H_{ox} (this study) are indicated with bars above the spectrum (carbonyl bands are dotted because their positions are not known from previous experiments and assumed to be shifted by 45 cm^{-1} compared to ^{12}CO-labeled H_{ox}). The blue areas indicate the probing region available by the lasers.

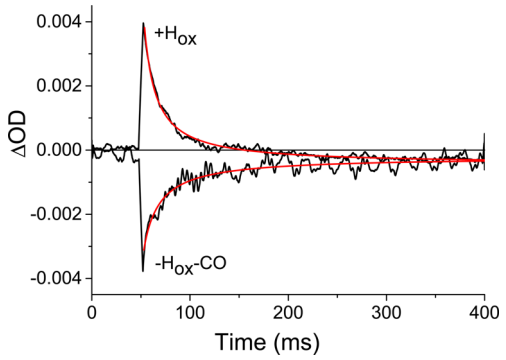

Figure 2. The 2.5 mM ^{13}CO-labeled CrHydA1 in the H_{ox}-CO-inhibited state. The kinetic trace is measured, from top to bottom, at 1895 cm^{-1}, showing the H_{ox} state formation and recarbonylation, and at 1770 cm^{-1}, showing the reversible bleach of the H_{ox}-CO band. Both are measured at room temperature (∼22 °C).

The kinetic traces fit better to a second-order decay (Figure 2) than to monoexponential kinetics (Figure S5), and the second-order rate constants vary between 1×10^5 and 4×10^5 M^{-1} s^{-1} for the different traces. A simple kinetic model where the CO is released to a nearby site and then geminately rebound at the active site would rather have displayed first-order kinetics. The CO rebinding must therefore be more complex, as is the case with myoglobin and cytochrome c.[29,30,33−37] CO may reach several sites with various rebinding rate constants, giving a multiexponential decay (that will be difficult to distinguish from a second-order decay), or possibly completely dissociate to the bulk solution, which could then give a true second-order rebinding. The recombination rate ($t_{1/2} \approx 13 \pm 5$ ms) compares well to similar rebinding experiments such as myoglobin−CO where the half-life for rebinding of CO at room temperature after photolysis is on the order of 10^2−10^3 ms or cytochrome c−CO with a rebinding time constant on the order of 10^1−10^3 ms at room temperature.[29,30,37]

CrHydA1 has been tested for hydrogen evolution and can reach TOFs of 500−1000 s^{-1}.[23] This means that each turnover is completed within 1−2 ms. This opens the way to use the photodissociation of the H_{ox}-CO state as trigger to start a catalytic cycle. The long lifetime of the H_{ox} state ($t_{1/2} \approx 13 \pm 5$ ms) determined here means that this catalytically active species has time to complete several catalytic cycles before it is inhibited, even in the presence of free CO at ambient temperature.

The present experiments show that time-resolved studies of catalytic intermediates of [FeFe] hydrogenases are possible using nanosecond laser flash/mid-IR probe spectroscopy. This opens the way for further studies where laser flash dissociation of CO can be a trigger for a H_2 molecule to enter the catalytic cycle and allows identification of further active site intermediates and the kinetics of their interconversion.

EXPERIMENTAL METHODS

The gene for the unmaturated CrHydA1 was overexpressed in *E. coli* strain BL21(DE3) ΔiscR with a pET21(b) plasmid containing the codon-optimized HydA gene with an N-terminal strep-II-tag and TEV cleavage site. Bacteria were grown

DOI: 10.1021/acs.jpclett.6b01316
J. Phys. Chem. Lett. 2016, 7, 3290−3293

according to Kuchenreuther et al.[21] but without coexpression of maturases and without any sodium fumarate. The LB contains 100 mg/L ampicillin, 30 mg/L kanamycin, 2 mM ferric ammonium citrate, 5 g/L glucose, 3.5 mM cysteine, and 0.5 mM of the inductor IPTG for the 20 h anaerobic expression at room temperature. After affinity chromatography purification, the strep-II-tag was cleavaged overnight by His_6-tagged TEV protease, which was finally removed. The unmatured protein was diluted to 250 μM in 25 mM Tris, 25 mM KCl, pH 8.0, and activated for 1 h at room temperature with an excess of $[Fe_2(adt)(CO)_4(CN)_2]^{2-}$. After removal of the excess complex, CrHydA1-adt was concentrated to 2.5 mM.

For room-temperature (~22 °C) transient absorption measurements, a frequency-tripled Q-switched Nd:YAG laser (Quanta-Ray ProSeries, Spectra-Physics) was employed to obtain 355 nm pump light with 50 mJ/pulse and a fwhm of 10 ns. Probing was done with two continuous-wave quantum cascade (QC) IR lasers with a tuning capability between 1765 and 1925 cm^{-1} for laser 1 and 1960 and 2150 cm^{-1} for laser 2 (Daylight Solutions). For IR detection, a liquid-nitrogen-cooled mercury−cadmium−telluride (MCT) detector (KMPV10-1-J2, Kolmar Technologies, Inc.) was used.

The IR probe light was superimposed on the actinic laser beam in a quasi-collinear arrangement at an angle of 25°. Transient absorption traces were acquired with a Tektronix TDS 3052 500 MHz (5GS/s) oscilloscope in connection with the L900 software (Edinburgh Instruments) and processed using Origin 9 software. Samples were kept in a home-built IR cell with CaF_2 windows using a Teflon spacer with a path length of 50 μm. All samples were prepared in an Ar-filled wet glovebox (Unilab, MBraun).

Infrared steady-state spectra were collected on a Bruker IFS 66v/S FTIR spectrometer controlled with OPUS software with a liquid-nitrogen-cooled MCT detector from Kolmar Technologies. The resolution of all measurements was 2 cm^{-1}, and the apodization function used was the Blackman−Harris three-term.

The quantum yield (ϕ) is calculated by estimating the number of CO-photodissociated enzymes (N_{diss}) and dividing this value by the number of absorbed photons (N_{abs})

$$\phi = \frac{N_{diss}}{N_{abs}}$$

The number of photodissociated enzymes can be measured by looking at the bleaches of the transient signals (ΔAbs) to estimate the concentration by Lambert−Beer law and multiplying the concentration (c) by the excitation beam cross section area (A = 1 cm^2) and the path length of the cell (l = 50 μm)

$$c = \frac{\Delta Abs}{\varepsilon l}$$

and

$$N_{diss} = N_A c A l$$

yields

$$N_{diss} = \frac{N_A A \Delta Abs}{\varepsilon}$$

where ε is the extinction coefficient at the wavenumber of the bleached band in question and N_A is the Avogadro constant.

The number of photons (N_{pho}) can be calculated by measuring the excitation pulse energy (E = 50 mJ) and calculating the number of photons in the pulse by knowing that all photons have a wavelength (λ) of 355 nm

$$N_{pho} = \frac{E\lambda}{hc_{light}}$$

where h is the Planck constant and c_{light} is the speed of light. The number of absorbed photons can be determined by knowing the absorbance of the sample at 355 nm (Abs)

$$N_{abs} = N_{pho}(1 - 10^{-Abs}) = \frac{E\lambda(1 - 10^{-Abs})}{hc_{light}}$$

Therefore, the quantum yield is then

$$\phi = \frac{N_{diss}}{N_{abs}} = \frac{hc_{light}N_A A \Delta Abs}{E\lambda\varepsilon(1 - 10^{-Abs})}$$

The fit equation for the second-order decays in Figure S4 is

$$y = \frac{[A]_0}{1 + [A]_0 k(x - t_0)} + b$$

where $[A]_0$, k, t_0, and b are constants corresponding to the initial absorbance at time zero, the second-order rate constant, time zero, and a background offset, respectively.

The fit equation for the monoexponential decays in Figure S5 is

$$y = [A]_0 e^{-(x-t_0)/\tau} + b$$

where $[A]_0$, τ, t_0, and b are constants corresponding to the initial absorbance at time zero, the lifetime of the process, time zero, and a background offset, respectively.

The three ratios between the χ^2 values of the monoexponential (first-order) fits and the second-order fits for the 1811, 1968, and 2013 cm^{-1} wavenumbers are 1.8, 2.0, and 0.52 respectively. This means that the second-order fits for two out of three decay traces are better than the monoexponential (first-order) fits.

■ ASSOCIATED CONTENT

Supporting Information

The Supporting Information is available free of charge on the ACS Publications website at DOI: 10.1021/acs.jpclett.6b01316.

Additional FTIR and UV−vis spectra and transient IR traces (PDF)

■ AUTHOR INFORMATION

Corresponding Authors

*E-mail: leif.hammarstrom@kemi.uu.se (L.H.).
*E-mail: wolfgang.lubitz@cec.mpg.de (W.L.).

Author Contributions

▽M.M and A.A.-V. contributed equally to this work.

Notes

The authors declare no competing financial interest.

■ ACKNOWLEDGMENTS

The authors are grateful for funding from the Knut and Alice Wallenberg Foundation, the Swedish Energy Agency, the Swedish Research Council, and the Max Planck Society.

DOI: 10.1021/acs.jpclett.6b01316
J. Phys. Chem. Lett. 2016, 7, 3290−3293

REFERENCES

(1) Frey, M. Hydrogenases: Hydrogen-Activating Enzymes. *ChemBioChem* **2002**, *3*, 153−160.
(2) Lubitz, W.; Ogata, H.; Rüdiger, O.; Reijerse, E. Hydrogenases. *Chem. Rev.* **2014**, *114*, 4081−4148.
(3) Magnuson, A.; Anderlund, M.; Johansson, O.; Lindblad, P.; Lomoth, R.; Polivka, T.; Ott, S.; Stensjö, K.; Styring, S.; Sundström, V.; Hammarström, L. Biomimetic and Microbial Approaches to Solar Fuel Generation. *Acc. Chem. Res.* **2009**, *42*, 1899−1909.
(4) Fontecilla-Camps, J. C.; Volbeda, A.; Cavazza, C.; Nicolet, Y. Structure/Function Relationships of [NiFe]-and [FeFe]-hydrogenases. *Chem. Rev.* **2007**, *107*, 4273−4303.
(5) Tard, C.; Pickett, C. J. Structural and Functional Analogues of the Active Sites of the [Fe]-,[NiFe]-, and [FeFe]-hydrogenases. *Chem. Rev.* **2009**, *109*, 2245−2274.
(6) Siegbahn, P. E.; Tye, J. W.; Hall, M. B. Computational Studies of [NiFe] and [FeFe] Hydrogenases. *Chem. Rev.* **2007**, *107*, 4414−4435.
(7) Wang, M.; Chen, L.; Sun, L. Recent Progress in Electrochemical Hydrogen Production with Earth-Abundant Metal Complexes as Catalysts. *Energy Environ. Sci.* **2012**, *5*, 6763−6778.
(8) Hambourger, M.; Gervaldo, M.; Svedruzic, D.; King, P. W.; Gust, D.; Ghirardi, M.; Moore, A. L.; Moore, T. A. [FeFe]-Hydrogenase-Catalyzed H2 Production in a Photoelectrochemical Biofuel Cell. *J. Am. Chem. Soc.* **2008**, *130*, 2015−2022.
(9) Camara, J. M.; Rauchfuss, T. B. Combining Acid−Base, Redox and Substrate Binding Functionalities to Give a Complete Model for the [FeFe]-Hydrogenase. *Nat. Chem.* **2011**, *4*, 26−30.
(10) Pullen, S.; Fei, H.; Orthaber, A.; Cohen, S. M.; Ott, S. Enhanced Photochemical Hydrogen Production by a Molecular Diiron Catalyst Incorporated into a Metal−Organic Framework. *J. Am. Chem. Soc.* **2013**, *135*, 16997−17003.
(11) Mulder, D. W.; Shepard, E. M.; Meuser, J. E.; Joshi, N.; King, P. W.; Posewitz, M. C.; Broderick, J. B.; Peters, J. W. Insights into [FeFe]-Hydrogenase Structure, Mechanism, and Maturation. *Structure* **2011**, *19*, 1038−1052.
(12) Brown, K. A.; Wilker, M. B.; Boehm, M.; Dukovic, G.; King, P. W. Characterization of Photochemical Processes for H2 Production by CdS Nanorod−[FeFe] Hydrogenase Complexes. *J. Am. Chem. Soc.* **2012**, *134*, 5627−5636.
(13) Brown, K. A.; Dayal, S.; Ai, X.; Rumbles, G.; King, P. W. Controlled Assembly of Hydrogenase-CdTe Nanocrystal Hybrids for Solar Hydrogen Production. *J. Am. Chem. Soc.* **2010**, *132*, 9672−9680.
(14) Wang, F.; Wang, W.-G.; Wang, H.-Y.; Si, G.; Tung, C.-H.; Wu, L.-Z. Artificial Photosynthetic Systems Based on [FeFe]-Hydrogenase Mimics: the Road to High Efficiency for Light-Driven Hydrogen Evolution. *ACS Catal.* **2012**, *2*, 407−416.
(15) Lubner, C. E.; Knörzer, P.; Silva, P. J.; Vincent, K. A.; Happe, T.; Bryant, D. A.; Golbeck, J. H. Wiring an [FeFe]-Hydrogenase with Photosystem I for Light-Induced Hydrogen Production. *Biochemistry* **2010**, *49*, 10264−10266.
(16) Esper, B.; Badura, A.; Rögner, M. Photosynthesis as a Power Supply for (Bio-) Hydrogen Production. *Trends Plant Sci.* **2006**, *11*, 543−549.
(17) Armstrong, F. A.; Evans, R. M.; Hexter, S. V.; Murphy, B. J.; Roessler, M. M.; Wulff, P. Guiding Principles of Hydrogenase Catalysis Instigated and Clarified by Protein Film Electrochemistry. *Acc. Chem. Res.* **2016**, *49*, 884−892.
(18) Hunt, N. T.; Wright, J. A.; Pickett, C. Detection of Transient Intermediates Generated from Subsite Analogues of [FeFe] Hydrogenases. *Inorg. Chem.* **2016**, *55*, 399−410.
(19) Vincent, K. A.; Parkin, A.; Armstrong, F. A. Investigating and Exploiting the Electrocatalytic Properties of Hydrogenases. *Chem. Rev.* **2007**, *107*, 4366−4413.
(20) Chen, Z.; Lemon, B. J.; Huang, S.; Swartz, D. J.; Peters, J. W.; Bagley, K. A. Infrared Studies of the CO-Inhibited Form of the Fe-Only Hydrogenase from Clostridium pasteurianum I: Examination of its Light Sensitivity at Cryogenic Temperatures. *Biochemistry* **2002**, *41*, 2036−2043.
(21) Kuchenreuther, J. M.; Grady-Smith, C. S.; Bingham, A. S.; George, S. J.; Cramer, S. P.; Swartz, J. R. High-Yield Expression of Heterologous [FeFe] Hydrogenases in Escherichia coli. *PLoS One* **2010**, *5*, e15491.
(22) Berggren, G.; Adamska, A.; Lambertz, C.; Simmons, T.; Esselborn, J.; Atta, M.; Gambarelli, S.; Mouesca, J.; Reijerse, E.; Lubitz, W.; Happe, T.; Artero, V.; Fontecave, M. Biomimetic Assembly and Activation of [FeFe]-Hydrogenases. *Nature* **2013**, *499*, 66−69.
(23) Esselborn, J.; Lambertz, C.; Adamska-Venkatesh, A.; Simmons, T.; Berggren, G.; Noth, J.; Siebel, J.; Hemschemeier, A.; Artero, V.; Reijerse, E.; Fontecave, M.; Lubitz, W.; Happe, T. Spontaneous Activation of [FeFe]-Hydrogenases by an Inorganic [2Fe] Active Site Mimic. *Nat. Chem. Biol.* **2013**, *9*, 607−609.
(24) Adamska, A.; Silakov, A.; Lambertz, C.; Rüdiger, O.; Happe, T.; Reijerse, E.; Lubitz, W. Identification and Characterization of the "Super-Reduced" State of the H-Cluster in [FeFe] Hydrogenase: A New Building Block for the Catalytic Cycle? *Angew. Chem., Int. Ed.* **2012**, *51*, 11458−11462.
(25) Adamska-Venkatesh, A.; Krawietz, D.; Siebel, J.; Weber, K.; Happe, T.; Reijerse, E.; Lubitz, W. New Redox States Observed in [FeFe] Hydrogenases Reveal Redox Coupling Within the H-Cluster. *J. Am. Chem. Soc.* **2014**, *136*, 11339−11346.
(26) Parkin, A.; Cavazza, C.; Fontecilla-Camps, J. C.; Armstrong, F. A. Electrochemical Investigations of the Interconversions between Catalytic and Inhibited States of the [FeFe]-Hydrogenase from Desulfovibrio desulfuricans. *J. Am. Chem. Soc.* **2006**, *128*, 16808−16815.
(27) Goldet, G.; Brandmayr, C.; Stripp, S. T.; Happe, T.; Cavazza, C.; Fontecilla-Camps, J. C.; Armstrong, F. A. Electrochemical Kinetic Investigations of the Reactions of [FeFe]-Hydrogenases with Carbon Monoxide and Oxygen: Comparing the Importance of Gas Tunnels and Active-Site Electronic/Redox Effects. *J. Am. Chem. Soc.* **2009**, *131*, 14979−14989.
(28) Baffert, C.; Demuez, M.; Cournac, L.; Burlat, B.; Guigliarelli, B.; Bertrand, P.; Girbal, L.; Léger, C. Hydrogen-Activating Enzymes: Activity Does Not Correlate with Oxygen Sensitivity. *Angew. Chem., Int. Ed.* **2008**, *47*, 2052−2054.
(29) Steinbach, P. J.; Ansari, A.; Berendzen, J.; Braunstein, D.; Chu, K.; Cowen, B. R.; Ehrenstein, D.; Frauenfelder, H.; Johnson, J. B. Ligand Binding to Heme Proteins: Connection between Dynamics and Function. *Biochemistry* **1991**, *30*, 3988−4001.
(30) Thielges, M. C.; Zimmermann, J.; Romesberg, F. E. Direct Observation of Ligand Dynamics in Cytochrome c. *J. Am. Chem. Soc.* **2009**, *131*, 6054−6055.
(31) Uhmann, W.; Becker, A.; Taran, C.; Siebert, F. Time-Resolved FT-IR Absorption Spectroscopy Using a Step-Scan Interferometer. *Appl. Spectrosc.* **1991**, *45*, 390−397.
(32) Greene, B. L.; Wu, C.-H.; McTernan, P. M.; Adams, M. W. W.; Dyer, R. B. Proton-Coupled Electron Transfer Dynamics in the Catalytic Mechanism of a [NiFe]-Hydrogenase. *J. Am. Chem. Soc.* **2015**, *137*, 4558−4566.
(33) Ansari, A.; Berendzen, J.; Braunstein, D.; Cowen, B. R.; Frauenfelder, H.; Hong, M. K.; Iben, I. E.; Johnson, J. B.; Ormos, P.; Sauke, T. B.; et al. Rebinding and Relaxation in the Myoglobin Pocket. *Biophys. Chem.* **1987**, *26*, 337−355.
(34) Henry, E. R.; Sommer, J. H.; Hofrichter, J.; Eaton, W. A.; Gellert, M. Geminate Recombination of Carbon Monoxide to Myoglobin. *J. Mol. Biol.* **1983**, *166*, 443−451.
(35) Frauenfelder, H.; Sligar, S. G.; Wolynes, P. G. The Energy Landscapes and Motions of Proteins. *Science* **1991**, *254*, 1598−1603.
(36) Schotte, F.; Lim, M.; Jackson, T. A.; Smirnov, A. V.; Soman, J.; Olson, J. S.; Phillips, G. N.; Wulff, M.; Anfinrud, P. A. Watching a Protein as it Functions with 150-ps Time-Resolved X-Ray Crystallography. *Science* **2003**, *300*, 1944−1947.
(37) Koutsoupakis, C.; Soulimane, T.; Varotsis, C. Ligand Binding in a Docking Site of Cytochrome c Oxidase: a Time-Resolved Step-Scan Fourier Transform Infrared Study. *J. Am. Chem. Soc.* **2003**, *125*, 14728−14732.

DOI: 10.1021/acs.jpclett.6b01316
J. Phys. Chem. Lett. 2016, 7, 3290−3293